Biology Faculty Research and Scholarship   Biology

10-2000

Linear and Nonlinear Measures Predict Swimming in the Leech

C. J. Cellucci

Peter Brodfuehrer
Bryn Mawr College, pbrodfue@brynmawr.edu

H. Acera-Pozzi

E. Dobrovolny

J. Engler

See next page for additional authors

Authors

C. J. Cellucci, Peter Brodfuehrer, H. Acera-Pozzi, E. Dobrovolny, J. Engler, R. Los, R. Thompson, and Alfonso M. Albano

Linear and nonlinear measures predict swimming in the leech

C. J. Cellucci,[1,3] P. D. Brodfuehrer,[2] R. Acera-Pozzi,[1] H. Dobrovolny,[1] E. Engler,[1] J. Los,[1] R. Thompson,[1] and A. M. Albano[1]

[1]*Department of Physics, Bryn Mawr College, Bryn Mawr, Pennsylvania 19010*
[2]*Department of Biology, Bryn Mawr College, Bryn Mawr, Pennsylvania 19010*
[3]*Department of Physics, Ursinus College, Collegeville, Pennsylvania 19426*
and The Arthur P. Noyes Clinical Research Center, Norristown, Pennsylvania 19401

Stimulation of a trigger interneuron of an isolated nerve cord preparation of the medicinal leech, *Hirudo medicinalis*, sometimes leads to swimming; sometimes it does not. We investigate signals transmitted in the ventral cord of the leech after stimulation and seek quantitative measures that would make it possible to distinguish signals that predict swimming from those that do not. We find that a number of linear as well as nonlinear measures provide statistically significant distinctions between the two kinds of signals. The linear measures are the time dependence of (i) the standard deviation and (ii) the autocorrelation function at a small time delay. The nonlinear measures are (i) a measure of nonlinear predictability and (ii) the time dependence of a measure of the size of the embedded signal trajectory. Calculations using surrogate data suggest that the differences between the two classes of signals are dynamical as well as statistical.

PACS number(s): 05.45.−a, 87.10.+e, 87.19.Nn

I. INTRODUCTION

In the medicinal leech, *Hirudo medicinalis*, the initiation of swimming following body wall stimulation can be traced, neuron to neuron, from the mechanosensory neurons that perceive the stimulus to motor neurons that produce the swimming movements [1–3]. In this swim-initiating pathway, neuronal information flows sequentially from mechanosensory neurons to trigger interneurons (cells Tr1), to segmental swim-gating interneurons, to oscillator interneurons. The output connections of the swim oscillator network drive motor neurons in each segmental ganglion that produce the undulatory body wall movements of swimming [1–3]. However, the synaptic interactions described in the swim-initiating pathway do not adequately explain the behavioral variability observed in the isolated leech nervous system following activation of this pathway. For example, stimulation of cell Tr1 can elicit swimming in one trial, but may not in the next trial, even though the strength of cell Tr1 stimulation is constant in both trials [3]. Similar behavioral variability also occurs in intact leeches in response to body wall stimulation [4].

Recent attempts to understand why stimulation of cell Tr1 does not reliably trigger swimming has led to the hypothesis that the control of swimming involves two parallel systems originating in the head ganglion that have opposite effects on the segmental swim-generating network, a swim-activating system that excites the segmental swim-generating network and a swim-inactivating system that inhibits or suppresses it [5]. In order for a given stimulus to initiate swimming, the swim-activating system must be turned on and the inactivating system turned off. Attempts to identify neurons in the head ganglion that comprise the swim-activating and -inactivating systems and are directly involved with determining whether a leech swims in response to a given stimulus have been largely unsuccessful [6]. The inability to physiologically identify individual neurons that strongly af-

fect the probability of eliciting swimming is consistent with the control of swimming being a function of the coordinated activity of large populations of neurons in the leech nervous system. Individual neurons may only make a small contribution to the net output of the system, and could easily be missed during physiological searches. Support for a distributed process controlling swimming is clearly revealed in extracellular records of neuronal spiking activity descending from the head ganglion in the lateral connectives prior to swimming. These recordings show a complex pattern of spiking activity that is coincident with the onset of swimming [5]. Collectively, these observations suggest that no single neuron or even a small group of neurons determines absolutely whether swimming will occur in response to a given input. Under these circumstances, a computational analysis of neuronal activity is most likely necessary to decipher how the leech nervous system encodes the initiation of swimming

One of the simplest things expected of the computational analysis of biological data is to provide some quantitative measures that would make it possible to distinguish distinct states of the system that produced the data. These states could be associated with different behaviors either as precursors or correlates of these behaviors. It is, however, not quite so easy to live up to these expectations. In recent years, for instance, various linear and nonlinear measures have been used to study human electroencephalograms (EEGs). Some of these studies have been attempts to forecast epileptic seizures ([7] and references therein, [8,9]). Although these have shown varying levels of promise there is, as yet, no reliable predictor of the onset of epilepsy [11,12].

Here, we explore the use of some linear and nonlinear techniques in the analysis of data from a simpler behavior in a much simpler system. We simply ask whether we can find quantitative measures that would make it possible to distinguish signals propagating in the leech ventral nerve cord that lead to swimming from those that do not. Specifically, we analyze two sets of time series measured from signals propagating along the ventral nerve cord following Tr1 stimula-
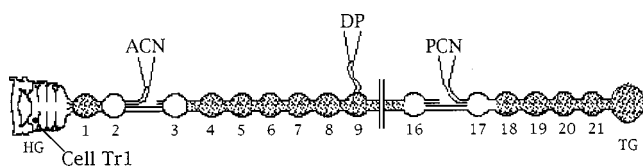
FIG. 1. Diagram of the experimental preparation. Preparation consists of the isolated leech ventral nerve cord extending from the head ganglion (HG) to the tail ganglion (TG). Extracellular recording of multiunit spiking activity in the lateral connectives were made at two locations: ACN, posterior to the segmental ganglion 2; PCN, anterior to segmental ganglion 17. Extracellular recording from a peripheral nerve (dorsal posterior, DP) was used to monitor the occurrence of swimming in the isolated nerve cord. Swimming was initiated by intracellular stimulation of cel Tr1.

tion. One signal propagates toward the rear while the other signal propagates toward the head (ACN and PCN, respectively, in Fig. 1). These signals are clearly nonstationary (see Fig. 2), so rather than using a single set of measures to describe an entire time series, or treating the signal's trajectory in a reconstructed state or phase space as an attractor, we partition it into successive nonoverlapping epochs and then use the time evolution of the properties of the epochs to characterize the time series.

We find that analysis of the ventral chord signals provides statistically significant discriminations between signals that lead to swimming and those that do not, and that these are achieved using both linear and nonlinear measures. The linear measures are the time dependence of the standard deviation and that of the autocorrelation function at some small time delay. The nonlinear measures are two that are relatively robust against noise and the limitations imposed by small data sets: (1) nonlinear predictablity [10,11], and (2) the time dependence of the mean distance between points in multidimensional time-delay embeddings of the data. In addition, we compare the patterns of spiking activity for swimming elicited by intracellular stimulation of cell Tr1 and swimming episodes that occur spontaneously.

II. NEURAL CORRELATES OF SWIMMING

1. Leech nervous system

The leech central nervous system consists of head and tail ganglia connected by the ventral nerve cord, a chain of 21 segmental ganglia and their intersegmental connectives. The segmental ganglia are numbered sequentially, from 1–21, beginning with the ganglion posterior to the head ganglion (Fig. 1). Each segmental ganglion is joined by connectives composed of two large lateral bundles of nerve fibers (2800 axons each) and a thin bundle called Faivre's nerve (97 axons) [13]). A pair of nerve roots arises from each segmental ganglion to innervate the body wall surrounding that segment. In isolated nerve cords, swimming activity is indicated by rhythmic bursts of action potentials in the dorsal posterior (DP) nerve, a branch of a segmental peripheral nerve [12].

2. Experimental setup

In an isolated leech nerve cord extending from the head ganglion to the tail ganglion, we recorded extracellularly
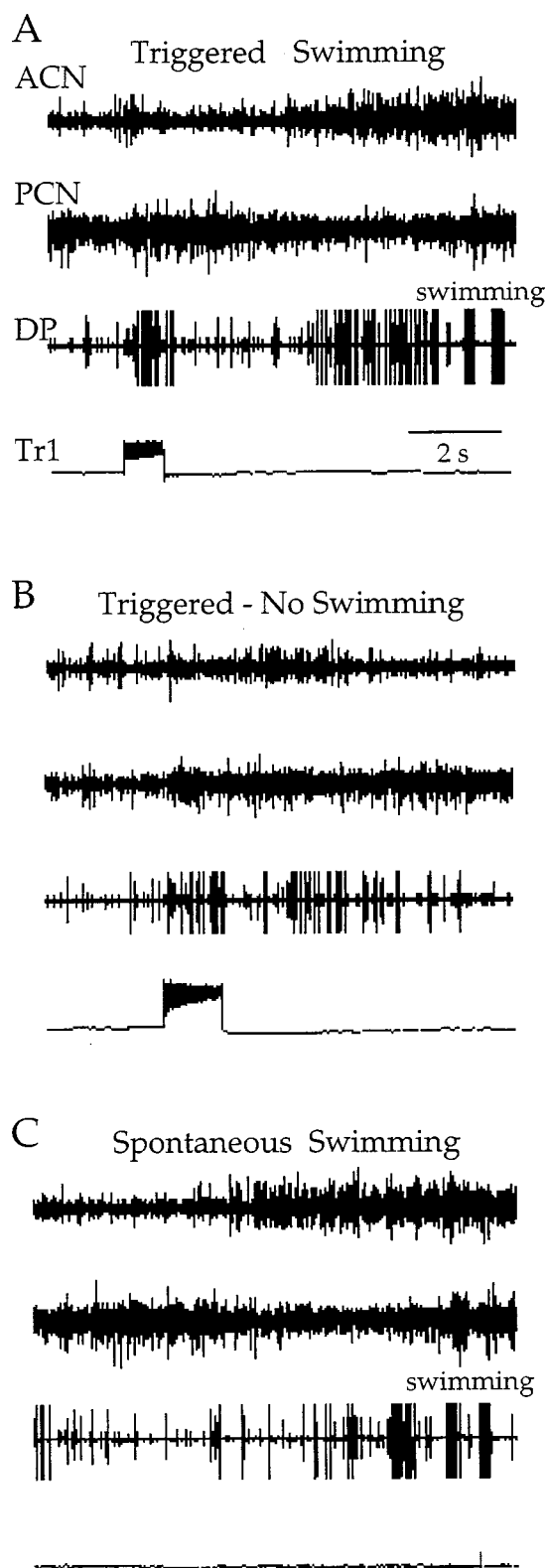

FIG. 2. Neuronal activity patterns in the lateral connectives associated with swimming and nonswimming trials. (a) and (c) In both triggered and spontaneous swim episodes, neuronal activity in ACN increases and decreases in PCN approximately 3 s before the initiation of swimming. (b) In nonswimming trials, no consistent change was evident in the activcity pattern in ACN or PCN.
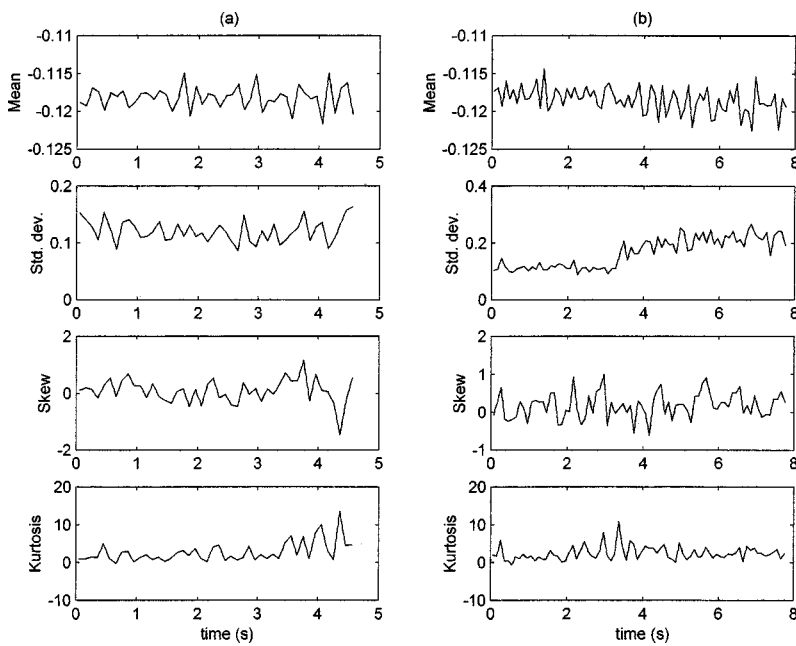
FIG. 3. Time dependence of the mean, standard deviation, skewness, and kurtosis of poststimulus ACN signals for (a) a nonswimming and (b) a triggered swimming case.

neural signals propagating in a lateral connective prior to and following stimulation of cell Tr1 (Fig. 1). Neuronal activity in the connectives and DP nerve was recorded using extracellular suction electrodes, while the electrical potential of cell Tr1 was recorded and stimulated using an Axoclamp 2B (Axon Instruments, Foster City, CA) amplifier in bridge mode. One extracellular recording location was from the cut end of one lateral connective posterior to segmental ganglion 2, (referred to as the anterior connective, ACN) while the other recording location was from the contralateral connective anterior to segmental ganglion 17 (posterior connective, PCN). Since the leech nervous system is bilaterally symmetrical, it is likely that the neural activity patterns recorded in one lateral connective reflect the spike activity patterns occurring in the other connective. The only noticeable difference between isolated preparations with intact lateral connectives and those with one lateral connective severed was an increase in the latency between Tr1 stimulation and the beginning of swimming in the latter group.

3. Physiological data

In the preparation described above, seven Tr1 stimulation trials triggered swimming and seven ''spontaneous'' swim episodes occurred. In all seven trials where stimulation of cell Tr1 triggered swimming, we observed two consistent changes in the neuronal activity pattern recorded from the anterior and posterior connective recording sites, ACN and PCN, respectively. First, several seconds prior to swimming, the amount and amplitude of neural signals in ACN increased and remained elevated throughout the duration of the swim episode. Second, coincident with the increase in ACN activity, large amplitude signals ceased and there was an overall decrease in neural activity in PCN that gradually increased before the onset of swimming [Fig. 2(a)]. An almost identical change in ACN and PCN activity patterns occurred before the onset of all seven spontaneous swim episodes: an increase in ACN activity and a simultaneous decrease in PCN activity [Fig. 2(c)]. On the other hand, in 13 trials

where Tr1 stimulation did not lead to swimming, no consistent change was evident in ACN and PCN activity patterns [Fig. 2(b)].

III. ANALYSIS

All analyses were performed on a time series consisting of a segment of ACN and PCN recorded data. For Tr1, triggered swim episodes this segment, referred to as the poststimulus segment, consisted of the portion of the time series starting at the end of spiking activity in cell Tr1 to the onset of swimming, which is indicated by the first burst of action potentials in the DP nerve (see Fig. 2). In trials where Tr1 stimulation did not elicit swimming, the end of the poststimulus period occurred approximately 6 s after stimulation of cell Tr1, which corresponded to the average swim latency in trials where swimming occurred following stimulation of cell Tr1. Data segments starting approximately 6 s before the onset of swimming were used in the analyses of spontaneous swim episodes.

A. Statistical and spectral measures

Each time series of extracellularly recorded ACN and PCN signals is partitioned into non-overlapping 400-point (0.100 s) epochs and linear measures are calculated for each epoch. This provides time-dependent characterizations of the time series. Figure 3 shows the time dependence of the mean, standard deviation, skewness, and kurtosis of poststimulus ACN signals for a nonswimming and a triggered swimming case. Figure 4 shows the same graphs for the ACN signal preceding a spontaneous swimming episode. Investigation of these figures and similar figures shows that only the standard deviations of the poststimulus ACN signals show any obvious differences—they increase before swimming starts. This is consistent with some of the qualitative observations made in the previous section.

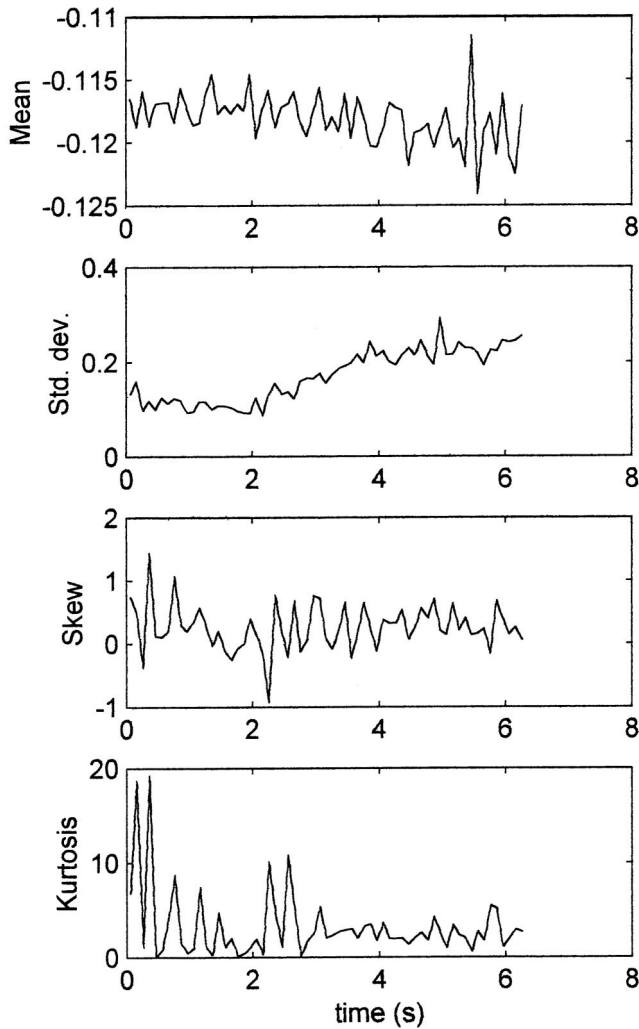A crude quantification of the time course of the signals may be obtained by performing a linear fit of their time

FIG. 4. Time dependence of the mean, standard deviation, skewness, and kurtosis of poststimulus ACN signals for a spontaneous swim episode.
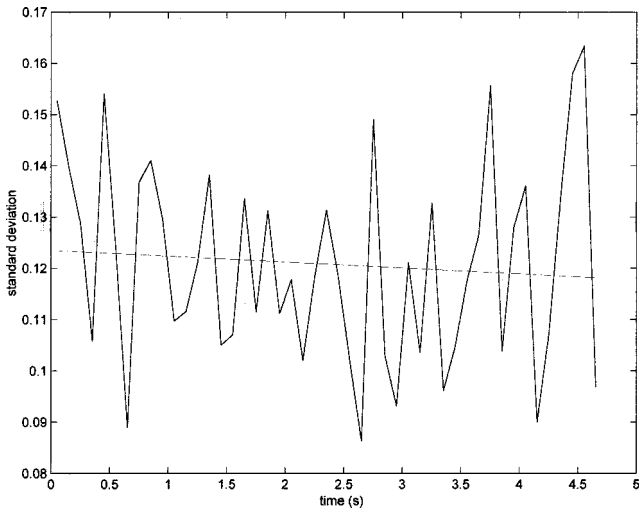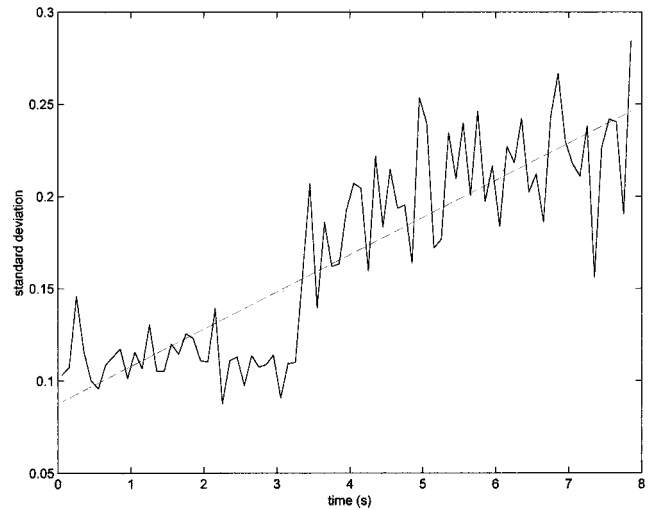

FIG. 6. Time dependence and linear fit (dashed line) of the standard deviation of a triggered swimming case.

dependence, and using the slopes of these fits to characterize the data. Figures 5 and 6 show the standard deviations vs. time, and the linear fits, for post-stimulus ACN signals corresponding to nonswimming and triggered swimming. Figure 7 shows the corresponding values for an ACN signal preceding spontaneous swimming. Figure 8 shows the slopes of these fits for all cases of each condition. The linear fits of all signals preceding swimming, triggered as well as spontaneous, have positive slopes. Eight of the 13 nonswimming cases do not.

Using a t test to compare the slopes, we find that the probability p that the post-stimulus nonswimming and triggered swimming ACN signals come from the same population is 9.3×10^{-7}. A similar comparison of the triggered swimming and spontaneous swimming signals gives $p = 0.015$; nonswimming vs spontaneous swimming gives $p = 2.2 \times 10^{-7}$. In contrast, a comparison of the poststimulus PCN nonswimming and triggered swimming signals gives $p = 0.51$. Although the slope does not give an unambiguous classification of each individual signal, it clearly provides a

FIG. 5. Time dependence and linear fit (dashed line) of the standard deviation of a nonswimming case.
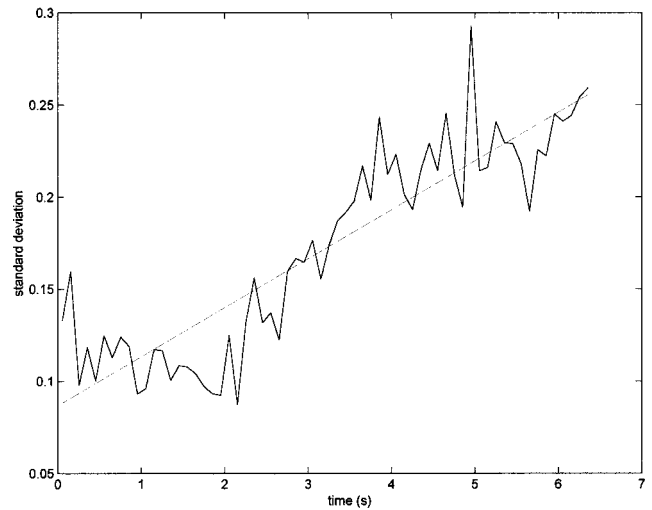

FIG. 7. Time dependence and linear fit (dashed line) of the standard deviation of a spontaneous swimming case.
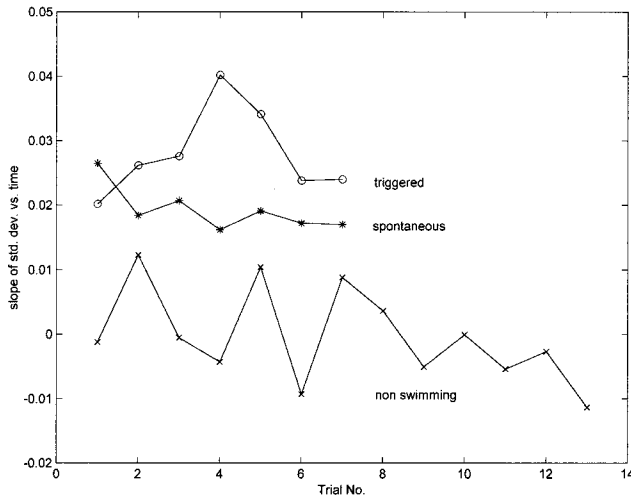
FIG. 8. Slopes of the linear fits of the time dependence of the standard deviation for all non-swimming, triggered swimming, and spontaneous swimming cases.

statistically significant distinction between the two classes of signals.

Figure 9 shows the time dependence of the power spectral densities (the Gabor transforms, see [14]) of an ACN signal after stimulation in (a) a case that did not lead to swimming and (b) one that led to swimming. Investigation of these and similar figures for the other data sets shows no obvious differences that could be used to distinguish one condition from the other. The autocorrelation function (Fig. 10) is the Fourier transform of the power spectral density (Wiener-Khinchin theorem, see, e.g., Ref. [15]), so one should convey the same information (or lack thereof) as the other. Nevertheless, despite the lack of easily identifiable global features that may be used to distinguish the signals, there are usable consistent differences in the time dependence of the autocorrelation function at small delays. Figure 11(a) shows the time dependence of the autocorrelation at a delay of 6 points (1.5 ms) for a poststimulus time signal that did not lead to swim-

ming; Figure 11(b) shows the time dependence of the autocorrelation for one that did.

As was done for the standard deviation, we show in Fig. 12 the slopes of linear fits of graphs such as Fig. 11 for all three conditions. t test comparisons of these values give $p = 8.8 \times 10^{-5}$ for nonswimming vs triggered swimming, $p = 2.1 \times 10^{-5}$ for nonswimming vs spontaneous swimming, and $p = 0.15$ for triggered vs spontaneous swimming.

B. Nonlinear measures

The standard deviation, like other measures based on statistical moments, depends only on the distribution of values and not on their time sequence. It is insensitive to dynamics. Some time sequence-dependent information is provided by spectra or autocorrelation functions, but this information can be mimicked by appropriately filtered noise [see, *e.g.*, Ref. [16] and Sec. III B 3 below]. In this section we investigate two nonlinear measures that are capable of eliciting some dynamical information from the data.

Traditional analyses of scalar time series such as those done in the preceding section focus their attention on one measured variable at a time. A system characterized by many coupled variables is more appropriately described by the simultaneous values of all the variables. These are represented by a point in the multidimensional state space spanned by the system's variables, and the system's dynamics is described by the trajectory of this representative state space point.

In situations when only values of a scalar quantity $\{x_1, x_2, \ldots, x_N\}$ are measured, the state space trajectory may be reconstructed in an m-dimensional state space by means of embedding vectors of the form [17–21],

$$X(n) = (x_n, x_{n+1}, \ldots, x_{n+m-1}). \tag{3.1}$$

Theorems by Takens [17] and Mañé [18] show that for a sufficiently large number of clean data, and if m is sufficiently large, the trajectory in the embedding space has the same geometric and topological properties as that in the original state space. In the following, we use the method of
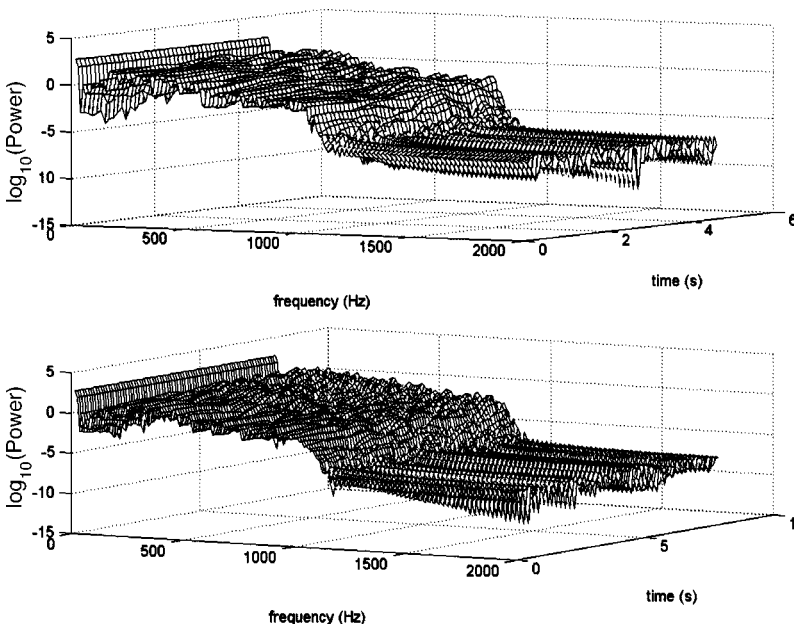

FIG. 9. Time dependence of the power spectral density (Gabor transform) of the poststimulus ACN signal for (a) a nonswimming case and (b) a triggered swimming case.
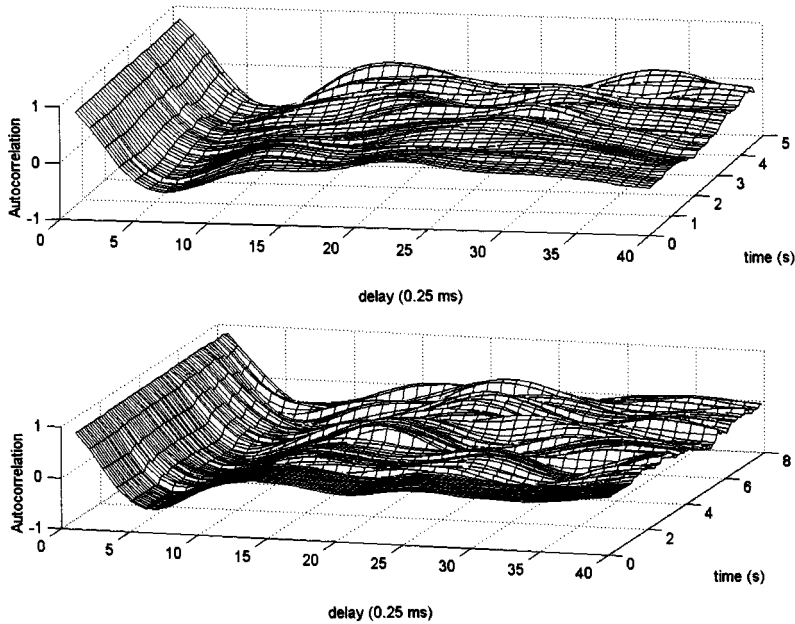
FIG. 10. Time dependence of the autocorrelation function of the poststimulus ACN signal for (top) a nonswimming case and (bottom) a triggered swimming case.

global false nearest neighbors and mutual information to determine embedding parameters [22].

1. Predictability

If a time series comes from a deterministic system then, in principle, it is possible to predict its future values from past ones. One technique that has been particularly effective is the use of local approximation [11]. In its simplest form, to predict $X(n+t)$ from $X(n)$, we look for that past state $X(n')$, with $n'<n$, that is closest to $X(n)$. We then determine where $X(n')$ is t time units later and use that state $[X(n'+t)]$ as the prediction for $X(n+t)$.

Our use of predictability differs from our use of the other measures in that we calculate a value that characterizes an entire time series rather than a sequence of values that tracks its time dependence. We take nonstationarity into account by using a moving window for the prediction. That is, to predict

$X(n+1)$, we start by locating $X(n)$'s nearest neighbor $X(n')$ from among the previous 2500 vectors, $X(n-2500)$, $X(n-2499)$, . . . ,$X(n-1)$. We then take as our prediction, $X^p(n+1)=X(n'+1)=(x_{n'},x_{n'+1}, \ldots, x_{n'+m-1})$. This is done for $n=2501$ until the end of the time series.

As a measure of the predictability, we use the root-mean-square (RMS) difference between the predicted and actual values scaled to the signal standard deviation. We used the median value of the RMS errors to compare time series since it is much less sensitive to outliers. In Fig. 13 we see a large difference between the predictability of ACN and PCN signals in the cases that did not lead to swimming. This difference is not as pronounced in the triggered and spontaneous swimming cases (Fig. 14). Since we cannot ascribe a significance to isolated values of the median prediction error for the individual signals, we use the differences between the ACN
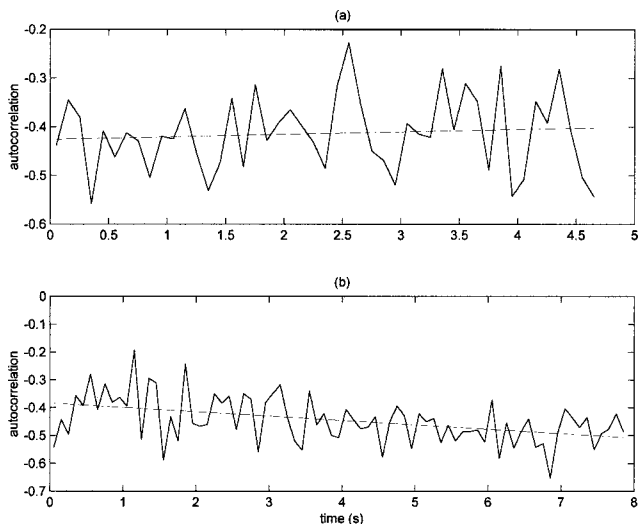

FIG. 11. Time dependence of the autocorrelation function for a time delay of 6 time units (1.5 ms) for (a) a nonswimming case and (b) a triggered swimming case.
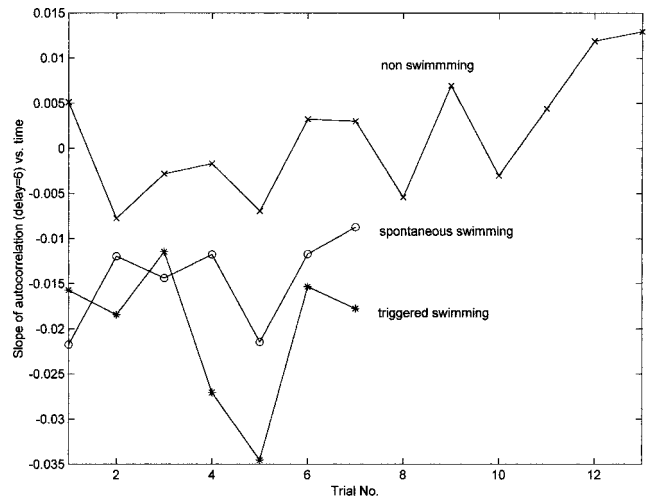

FIG. 12. Slopes of the linear fits of the time dependence of the autocorrelation function for a time delay of 6 time units (1.5 ms) for all nonswimming, triggered swimming, and spontaneous swimming cases.
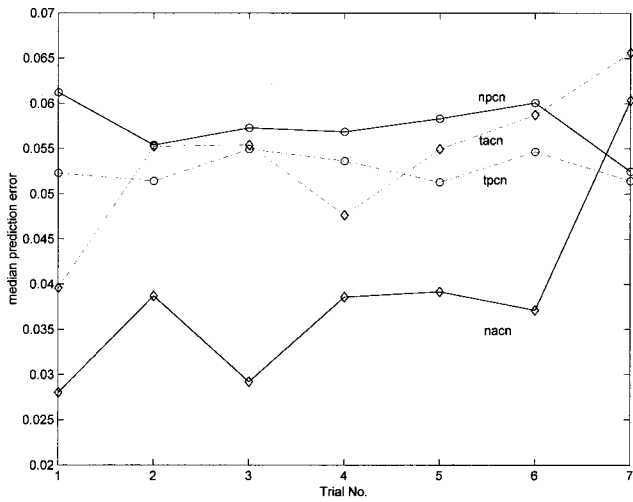
FIG. 13. Median prediction errors for poststimulus nonswimming (nacn and npcn) and triggered (tacn and tpcn) swimming signals.

and PCN values to compare the different cases. Using a paired t test, we find that the probability that the poststimulus nonswimming ACN and PCN are equally predictable is $p = 9.3 \times 10^{-3}$. The corresponding probabilities for the triggered swimming and spontaneous swimming cases are 0.75 and 0.16, respectively. In the nonswimming case, the concurrent ACN and PCN signals differ significantly in predictability; in the swimming cases, they do not.

2. Mean interpoint distance

For this measure we use a very simple characterization of the embedded trajectory, namely the average distance $\langle r \rangle$, between embedded vectors. We use $\langle r \rangle$ to investigate the time evolution of the ACN and PCN signals individually as separate univariate data, as well as together as elements of a bivariate data set. In the former case, we form m-dimensional embeddings using each signal separately; in the latter case, we use values of both ACN and PCN in the embedding.

Figure 15(a) shows the $\langle r \rangle$ vs time graph for an ACN
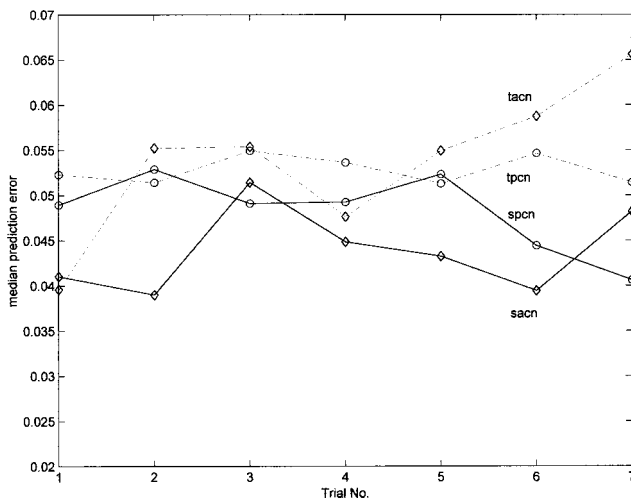

FIG. 14. Median prediction errors for poststimulus triggered (tacn and tpcn) and spontaneous (sacn and spcn) swimming signals.
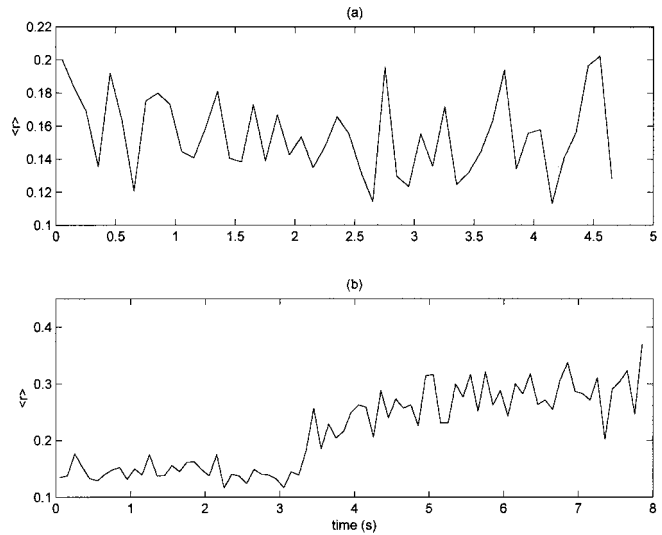

FIG. 15. Mean interpoint distance $\langle r \rangle$, vs time for (a) a nonswimming and (b) a triggered swimming ACN signal embedded in two dimensions.

signal embedded in two dimensions in a nonswimming case. Figure 15(b) shows a triggered swimming case. Slopes of the linear fits of the time dependence of $\langle r \rangle$ for all data sets are shown in Fig. 16. All signals that preceded swimming, whether triggered or spontaneous, are characterized by positive slopes. All but 3 of the 13 nonswimming signals have negative slopes. t-test comparisons show that the probability, p, that the 13 nonswimming and the 7 triggered swimming ACN signals come from the same population is 1.5×10^{-4}. The distinction is even sharper in higher embedding dimensions (a five-dimensional calculation gives $p = 3.2 \times 10^{-6}$).

To compare the time evolution of the ACN and PCN signals as separate univariate data with their behavior as elements of a bivariate data set, we combine the first seven nonswimming trials with the seven swimming trials. Figure
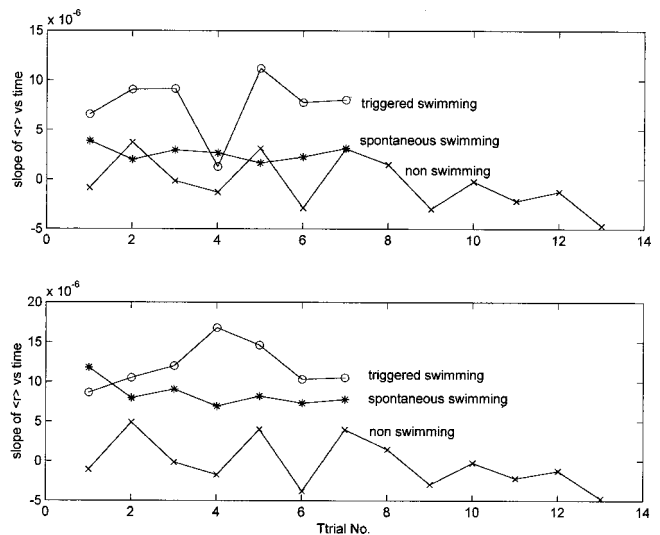

FIG. 16. Slopes of the linear fits of the time dependence of $\langle r \rangle$ for all non-swimming, triggered swimming, and spontaneous swimming cases for embedding dimension = 2 (top), and embedding dimension = 5 (bottom).
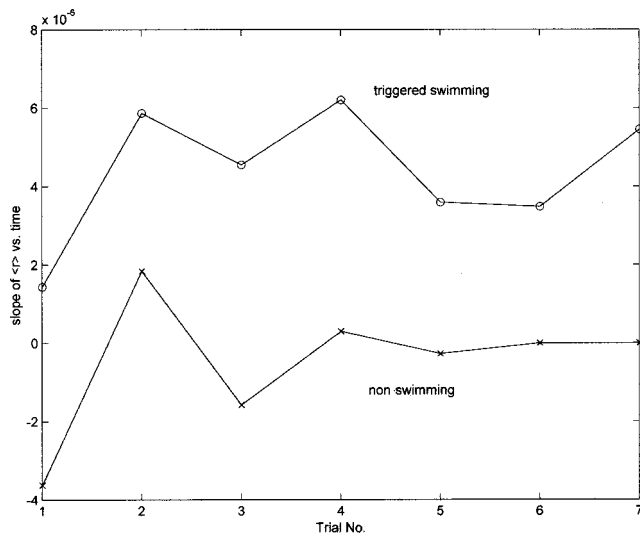
FIG. 17. Slopes of the linear fits of the time dependence of $\langle r \rangle$ for nonswimming and triggered swimming using simultaneous values of the ACN and PCN signals as coordinates of a two-dimensional embedding.

17 shows results obtained by using simultaneous values of the ACN and PCN signals as coordinates of a two-dimensional embedding. A t-test comparison of the first seven ACN nonswimming signals with the seven triggered swimming signals gives $p = 8.2 \times 10^{-4}$. A similar comparison of the PCN signals gives $p = 0.54$, indicating that the PCN signals in the nonswimming and triggered swimming cases are indistinguishable. Nevertheless, comparing the results shown in Fig. 17 in which we use a two-dimensional embedding using both ACN and PCN signals gives $p = 1.7 \times 10^{-4}$, a slightly better discrimination than that obtained using just the ACN signal. This suggests some correlation between the two data streams, but not enough to make more than an insignificant difference. Using a six-dimensional embedding gives a slightly worse discrimination, with $p = 4.4 \times 10^{-4}$.

3. Surrogate data and dynamical information.

Results obtained above using the standard deviation depend only on statistical information that is insensitive to the time order of the data. Differences found using nonlinear predictability and mean interpoint distance suggest that there may be dynamical differences as well. Here we use surrogate data to seek further corroboration of the presence of dynamical differences.

The method of surrogate data has become an important tool for dynamical analysis [16,23–25]. Given a data set, the method consists of creating other data sets that share some properties of the original but which are otherwise random. Similarities, or lack thereof, of the values of dynamical measures applied to the original and to the surrogates are then used to test the null hypothesis that the original data belong to the same class of random data as the surrogates.

The two types of surrogates we use are (1) a random shuffle of the elements of each epoch, and (2) a phase-randomized surrogate of each epoch. The latter is obtained

by calculating the finite Fourier transform of the original data, randomizing the phases of the transform, symmetrizing the randomized transform to assure a real inverse, and then taking the inverse transform to generate the surrogate [19]. Shuffled surrogates have the same distributions and therefore the same standard deviations as the originals. Random phase surrogates have the same power spectral densities (and therefore the same autocorrelations) but not the same standard deviations. Thus, for instance, a t-test comparison of the autocorrelation functions (at delay 6) of the ACN nonswimming data with a single shuffled surrogate data set gives $p = 0.33$, while a similar comparison with a random phase surrogate gives $p = 0.93$.

To study how surrogate data affect the behavior of $\langle r \rangle$, each ACN signal is partitioned into nonoverlapping 400-point epochs as above. Each epoch is used to generate a surrogate and the time dependence of $\langle r \rangle$ is calculated in five dimensions for the sequence of surrogate epochs. The procedure is implemented five times for each of the two types of surrogates. A paired t-test comparison of the slopes of the $\langle r \rangle$ vs time curves for the nonswimming ACN signals with the averages of their shuffled surrogates gives $p = 0.66$ while a similar comparison of the triggered swimming ACN signals gives $p = 8.6 \times 10^{-5}$. The corresponding values for comparisons with random phase surrogates are $p = 0.46$ for nonswimming and $p = 2.5 \times 10^{-5}$ for triggered swimming. A comparison using spontaneous swimming gives $p = 1.37 \times 10^{-5}$ for shuffled data and $p = 1.75 \times 10^{-5}$ for random phase surrogates. These results suggest the absence of dynamical information in the signals that do not lead to swimming and their presence in signals that do lead to swimming. The statistical differences, which are significant, between the original triggered swimming signals and their surrogates indicate that there is information in the original that is destroyed in the process of creating the surrogates even if these surrogates preserved the standard deviation in one case and the power spectrum in the other.

IV. CONCLUDING REMARKS

The physiological observations show that both the ACN and PCN signals behave differently when the leech is about to swim from when it is not. The discrimination between signals that precede swimming from those that do not can be made in a statistically significant manner using linear as well as nonlinear dynamical measures. Surprisingly, this can be done more clearly for ACN than for PCN signals. These measures, however, can only distinguish different classes; they do not unambiguously classify individual signals. Use of surrogate data suggests that the two classes of signals differ not only statistically, but dynamically as well.

Using linear fits to characterize time dependence is an oversimplification that is clearly insensitive to much of the complexity of the computed measures. This oversimplification may underlie the inability to identify statistical differences between PCN signals. More sophisticated analysis would likely reveal details that may enable unambiguous classification of individual signals or lead more directly to the underlying biology.

Even with these limitations, the linear and nonlinear

analyses, along with the analysis of surrogate data, highlight the importance of understanding the temporal characteristics of neuronal activity in the leech ventral nerve cord to determine the underlying physiology controlling swim initiation. Changes in the total amount of activity in the nerve cord, although important, clearly do not adequately describe the pattern of neuronal activity in the leech nerve cord that predicts whether a given stimulus will initiate swimming.

[1] P. D. Brodfuehrer and W. O. Friesen, Science **234**, 1002 (1986).

[2] W. O. Friesen, in *Neuronal and Cellular Oscillators*, edited by J. W. Jacklet (Dekker, New York, 1989).

[3] P. D. Brodfuehrer, E. A. Debski, B. A. O'Gara, and W. O. Friesen, J. Neurobiol. **27**, 403 (1995).

[4] W. B. Kristan, Jr., S. J. McGirr, and G. V. Simpson, J. Exp. Biol. **96**, 143 (1982).

[5] P. D. Brodfuehrer and A. Burns, Neurobiol. Learn Mem. **63**, 192 (1995).

[6] P. D. Brodfuehrer (unpublished).

[7] K. Lehnertz and E. E. Elger, Phys. Rev. Lett. **80**, 5019 (1998).

[8] A. M. Albano, C. Bedonie, C. J. Cellucci, D.Halkides, V. Miller, J. Ree, A. Torruella, R. Harner, and P. E. Rapp, in *Nonlinear Dynamics and Brain Functioning*, edited by R. Sreenivasan, N. Pradhan, and P. E. Rapp (Nova Science, New York, 1999).

[9] M. Le Van Quyen, J. Martinerie, C. Adam, and F. J. Varela, Physica D **127**, 250 (1999).

[10] G. Sugihara and R. M. May, Nature (London) **344**, 734 (1994).

[11] J. D. Farmer and J. J. Sidorowich, Phys. Rev. Lett. **59**, 845 (1987).

[12] K. J. Muller, J. G. Nicholls, and G. S. Stent, *Neurobiology of the Leech* (Cold Spring Harbor Laboratory, Cold Spring Harbor, NY, 1981).

[13] J. M. Wilkinson and R. E. Coggeshall, J. Comp. Neurol. **162**, 387 (1975).

[14] D. Gabor, J. Inst. Electr. Eng., Part III **93**, 429 (1946).

[15] W. H. Press, B. P. Flannery, S. A. Teukolsky, and W. T. Vetterling, *Numerical Recipes: The Art of Scientific Computing*, 2nd ed. (Cambridge University Press, Cambridge, England, 1998).

[16] J. Theiler, J. Galdrikian, A. Longtin, S. Eubank, and J. D. Farmer, in *Nonlinear Modeling and Forecasting*, edited by M. Casdagli and S. Eubank (Addison-Wesley, Reading, MA, 1992).

[17] F. Takens, in *Dynamical Systems and Turbulence, Warwick, 1980*, edited by D. A. Rand and L. S. Young (Springer-Verlag, New York, 1981).

[18] R. Mañé, in *Dynamical Systems and Turbulence, Warwick 1980* (Ref. [17]).

[19] N. H. Packard, J. P. Crutchfield, J. D. Farmer, and R. S. Shaw, Phys. Rev. Lett. **45**, 712 (1980).

[20] J.-P. Eckmann and D. Ruelle, Rev. Mod. Phys. **57**, 617 (1985).

[21] T. Sauer, J. A. Yorke, and M. Casdagli, J. Stat. Phys. **65**, 579 (1991).

[22] M. Kennel, R. Brown, and H. D. I. Abarbanel, Phys. Rev. A **45**, 3403 (1992).

[23] J. Theiler and P. E. Rapp, Electromyogr. Clin. Neurophysiol. **98**, 213 (1996).

[24] P. E. Rapp, A. M. Albano, I. D. Zimmerman, and M. A. Jiménez-Montaño, Phys. Lett. A **192**, 27 (1994).

[25] T. Schreiber and A. Schmitz, Phys. Rev. Lett. **77**, 635 (1996)